Journal of Thermal Analysis, Vol. 37 (1991) 1223-1238

Dedicated to Professor Dr. H. J. Seifert on the occasion of his 60th birthday

THERMAL ANALYSIS STUDY OF THE INFLUENCE OF RAPID SOLIDIFICATION ON THE PRECIPITATION KINETICS OF THE δ' (Al_3Li) METASTABLE PHASE IN AN Al–Mn–Li ALLOY

J. Baram and A. N. Sembira***

*MATERIALS ENGINEERING DEPARTMENT,
**CHEMICAL ENGINEERING DEPARTMENT, BEN-GURION UNIVERSITY OF THE NEGEV, BEER-SHEVA, ISRAEL

(Received October 10, 1990)

The precipitation kinetics of the δ' (Al_3Li) phase in two rapidly solidified and one conventionally cast samples of an Al–2.3Li–6.5Mn (in wt%) alloy are compared. Following high cooling rates, manganese is retained in solid solution in the aluminium matrix (αAl) up to 6.0 wt%, far beyond the thermodynamic equilibrium value (0.36 wt% at 500°). Extended solid solution of manganese in aluminium induces strain gradients, similar to those produed by dislocations. The effect of such gradients, the size of which is proportional to the solute atomic fraction, is to enhance lithium precipitation, by lowering the activation energy, as observed, and also by affecting the rate parameter. Kinetic thermal analysis has been performed in a series of nonisothermal DTA experiments, operated in the heat flux DSC mode. The precipitation of the δ' (Al_3Li) phase is evidenced by an exothermic peak whose characteristics were analyzed. The rate of transformation (precipitation) is assumed to obey the Johnson–Mehl–Avrami equation. The activation energy for the precipitation process, as well as the kinetic rate parameter have been evaluated for the rapidly solidified and the conventionally cast specimens. The activation energy for precipitation is lowered, from 105 $kJ \cdot mol^{-1}$ for the conventionally cast material, down to 77 $kJ \cdot mol^{-1}$ for a sample that exhibits manganese solid solubility extension of 6.00 wt%. The rate parameter for the precipitation reaction is reduced from about 1.40 for the slowly cast sample to 1.20 the rapidly solidified sample, as a result of additional stress-assisted precipitation.

Aluminum alloys, as structural materials for aerospace structures, are subject to extensive research in the past and present years [1-3]. The objective of that research is to lower densities and increase strength. Lithium additions to an aluminum matrix provide a dramatic increase in elastic modulus indeed, 6% per each wt% Li added, and a significant decrease in density, 3% per each wt% lithium added. The stiffness improvement results

John Wiley & Sons, Limited, Chichester
Akadémiai Kiadó, Budapest

from solution of lithium in the aluminum matrix and from precipitation of Al_3Li dispersoid. The equilibrium solid solubility of lithium in aluminium is however limited. In order to increase that solubility beyond the equilibrium limit, rapid solidification (RS) techniques are beneficial in producing stable alloys, with extended lithium solid solubility [4]. Al–Li are age–hardenable alloys, with the following precipitation sequence: supersaturated solid solution → δ' (Al_3Li) → δ (AlLi). The δ' transition phase forms in spherical particles having and ordered $L1_2$ crystal structure [5]. Al–Li alloy have however shown low ductility and fracture toughness, due to strain localization effects within the Al–Li matrix, resulting either from planar slip associated with the sherable nature of the ordered δ' precipitates or to the presence of 'soft' precipitate free zones (PFZ) adjacent to grain boundaries. Refining the grain size and adding fine hard dispersoids provide a remedy to this ductility problem. The introduction of transition metals like manganese yields indeed grain refinement, inhibits recrystallization, and even improves corrosion resistance and mechanical properties at elevated temperatures. Manganese behaves as a dispersoid formation element through the Al_6Mn phase. The presence of the non-shearable Al_6Mn dispersoids, are effective in dispersing slip and alleviating the problem associated with planar slip. However, it has also been reported that manganese dispersoids promote the formation of the stable δ AlLi phase during aging, resulting in consequent degradation of the mechanical properties [6]. RS has the potential to remove that restriction by either directly generating a fine dispersion of intermetallic phases in the alumnium matrix, or by retaining a substantial proportion of the alloying element as an extended solid solution (manganese in aluminum) or eventually precipitating in a subsequent aging treatment.

In order to get insight on the precipitation mechanisms involved in the Al–Li–Mn alloy, and to check for the influence of the high cooling rate applied during rapid solidification, differential thermal analysis has been performed for the observation of the δ' (Al_3Li) phase formation. The kinetics of the precipitation process of as–atomized, i.e. rapidly solidified (RS), fine powders are compared to those of a conventionally cast ingot material (IM) of same alloy composition.

Experimental

In the present paper, we compare the precipitation sequence in 2 differently processed samples of an Al–2.3Li–6.5Mn (in wt%) alloy. One sample, labelled RS, consists of powder particulates produced by high pres-

sure argon gas atomization of the melt, sieved in the $<45\ \mu$m size fraction, all spherical in shape. Particle size analysis (by sedimentation) showed that about 60 wt% of that size fraction consisted of powders 10-20 μm in diameter. The argon gas pressure used for atomization was 50 atm. The second sample, labelled IM, is an as-cast specimen, of the same composition, obtained by conventional ingot metallurgy. The correlation between the secondary phases content in these specimens and the quenching rate practiced for their production has been discussed elsewhere [7-8].

The kinetic thermal analyses have been performed in a series of non-isothermal experiments with a Thermal Analysis Data Station (TADS) Perkin–Elmer DTA–1700 system, operated in the heat flux DSC mode. The samples were all 90-110 mg in weight, and the same weight of crystallized aluminum oxide powder served as reference. A built–in scanning autozero function was used for optimizing the instrumental baseline for each run. All measurements were carried out with alumina sample liner and argon purge gas flow of 50 $cc \cdot min^{-1}$. For the calculation of the precipitation kinetics, a computer program has been used [9]. The file of raw experimental data created by the TADS system is an input for the main program, and is converted in a new file as follows: the baseline is first extrapolated between the chosen lower (T_1) and the upper (T_2) temperatures; then α_i, the fraction of material reacted (precipitated) between T_1 and T_i and $(d\alpha / dt)_i$, the transformation (precipitation) rate are determined at selected temperatures T_i. These values serve as input for the calculation of the kinetic parameters, assuming a given kinetic model, as explained in the next section.

The kinetic model formulation

It is assumed that the effects of thermal inertia are negligibly small, that the transformation rate is proportional the heat evolution rate:

$$(d\alpha / dt)_i \approx (dQ/dt) \qquad [1]$$

where α is the fraction reacted (precipitated) and Q is the amount of heat evolved druing the reaction. The isothermal rate of the transformation is assumed to follow a kinetic equation of the form [9-10]:

$$\alpha(t) = 1 - \exp[-K(T)t^n] \qquad [2]$$

This is the well-known Johnson–Mehl–Avrami (JMA) equation, where t is time, n is the kinetic rate parameter for the transformation and $K(T)$ is a temperature dependent rate constant in the Arrhenius form [11-12]:

$$K(T) = A \cdot \exp\left[-\frac{E}{RT}\right] \qquad [3]$$

where R is the gas constant, T the temperature and E the so-called 'activation energy' for the process involved (the precipitation of the δ' (Al_3Li) phase in the Al–Li–Mn alloy). The preexponential term A is taken as temperature-independent. The suitability of the assumption that the JMA equation holds for the precipitation process under investigation has to be assessed (see below).

The DTA runs conducted in this experiment are not isothermal. It has however been shown [13-15] that the formalism developed for the study of the kinetics in isothermal conditions, can be adapted to non-isothermal processes, mainly in solids-tate reactions, where nucleation and/or growth of the product phase do occur.

The time derivative of the fraction reacted is:

$$\frac{d\alpha}{dt} = K^{1/n} n (1-\alpha)\left[-\ln(1-\alpha)\right]^{(n-1)/n} \equiv K^{1/n} g(\alpha) \qquad [4]$$

For non-isothermal DSC experiments, at various heating rates β, the following holds:

$$\frac{d\alpha}{dT} = \frac{1}{\beta} \cdot \frac{d\alpha}{dt} \qquad [5]$$

After some elementary algebraic manipulation, one gets:

$$y(\alpha) = \frac{d\alpha}{dT} = \frac{A^{1/n}}{\beta} \cdot \exp\left[-\frac{E}{nRT}\right] g(\alpha) \qquad [6]$$

The term E/n is calculated using the method developed by Kissinger [16-17] from graphs of the logarithm of the heating rate *vs.* inverse temperature

at the maximum of the reaction rate in constant heating rate DSC experiments:*

$$\frac{d\left[\ln\left(\frac{\beta}{T_p^2}\right)\right]}{d\left(T^{-1}\right)} = -\frac{E}{nR} + Ct \qquad [7]$$

where T_p is the temperature at which the heat evolved is maximum.

The practiced procedure is now to obtain the values for α from the heating runs, and then compute:

$$\left[\frac{d\alpha}{dT}\right] \cdot \exp\left[\frac{E}{nRT}\right] = \frac{A^{1/n}}{\beta} \cdot g(\alpha) \qquad [8]$$

The right–side of Eq. [8] may have, or may not have a maximum, with respect to temperature. If there is such a maximum, and α_p is $\cong 0.633$ then the JMA model provides a suitable description of the process under study [18]. In that case, the rate parameter n is easily calculated:

$$n = \frac{1}{1 + \ln(1 - \alpha_M)} \qquad [9]$$

where α_M is the value of α for which the right-side part of Eq. [9] reaches its maximum. The pre-exponential factor A can be computed as well. Knowing the rate parameter value n, enables now the calculation of the activation energy E for the process.

Results and discussion

The morphology of the studied samples is shown in Fig. 1. Figure 1a1 is an electron microscope view of the RS powder material and Fig. 1a2, a polished and chemically etched section of a typical RS powder particle. Fig. 1b is an optical micrograph of the IM material (polished and chemically etched).

---

* The evaluation of the activation energy by using the Kissinger procedure, yields the term E/n and not E, as shown in Ref.[14]

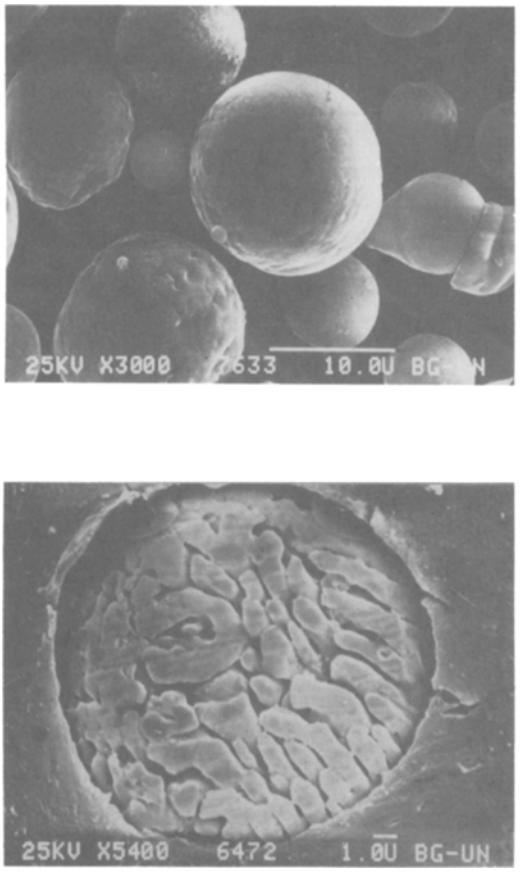

Fig. 1a Micrographs of: a) the RS sample, a1,–as–atomized; a2,–polished and etched; scanning electron micrographs

X–ray diffraction was performed on both samples to check for the presence of secondary phases, and for eventual extension of the solid solubility of manganese in aluminum, beyond the thermodynamic equilibrium limit, as is known to occur in rapidly solidified material [8]. In sample IM, the following secondary phases were identified: AlLi, Al_6Mn and Al_4Mn. In Fig. 1a, the 'coffin' morphology of the Al_4Mn phase is arrowed, as well as the 'puzzle pieces' morphology of the Al_6Mn phase [19]. The AlLi phase is finely dispersed in the aluminum matrix, and therefore not seen on the figure. In sample RS, a small amount of the Al_4Mn phase was detected (not enough to be seen on the micrograph 1a2). The estimation of the amount of manganese in metastable solid solution in the aluminum

matrix at room temperature was done by checking the lattice parameter change of aluminum by X–ray diffraction, using CuK_α radiation, through the dependence of the (331) aluminum interplanar spacing, d_{331}, on the manganese content [20]. The manganese solubility extent in the aluminum matrix has also been measured by Energy Dispersive Analysis of X–rays (EDAX), in a 20 kV scanning electron microscope, using a spot size of 100 nm and 30° tilt, with reference to pure aluminum and manganese as standards. Both methods did produce similar results, namely 6.0 wt%. The thermodynamic equilibrium values are: 1.82 wt% at the eutectic temperature 685.5°, 0.36 wt% at 500°. The RS sample did of course solidify rapidly, at a high quenching rate, computed to be $1.52 \cdot 10^5$ deg·sec^{-1} [21]. The IM sample is believed to have solidified at a rate of 10-100 deg·sec^{-1} only.

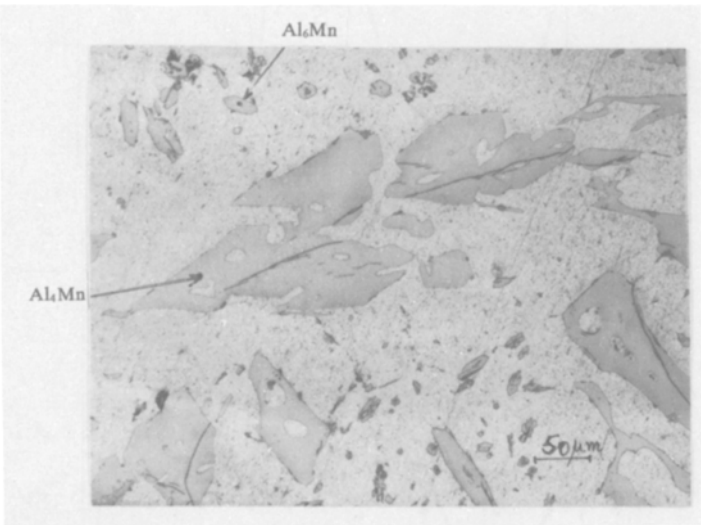

Fig. 1b Micrographs of: b) the IM sample morphology; notice the secondary phases; optical micrographs

Typical thermal curves of the studied samples, heated at 15 deg·min^{-1}, are shown in Figs 2a (the RS sample) and 2b (the IM sample). The exothermic peaks evolved from the precipitation of the δ' (Al_3Li) phase are labelled III. The other peaks observed in Figs 2 are attributed to additional solid state transformations occurring in the samples, such as the precipitation (labelled I) and dissolution (labelled II) of an AlLi phase which is metastable with respect to δ' (probably analogue to Guinier–Preston, 'GP', zones in Al–Cu alloys [22]), and occurs at low temperatures (between 80°

and 140°); the dissolution of δ' [1-2], between 202° and 277° (labelled IV); the precipitation of the δ (AlLi) phase (labelled V); the dissolution (labelled VI, between 382° and 457°) of the δ phase [5, 23], and the decomposition of the Al_6Mn phase (labelled VII, between 440° and 540°) [24]. The dissolution of the δ' (Al_3Li) and the δ (AlLi) phases is also evidenced by an increase in heat capacity, as is clearly observed in both Figs 2. The con-

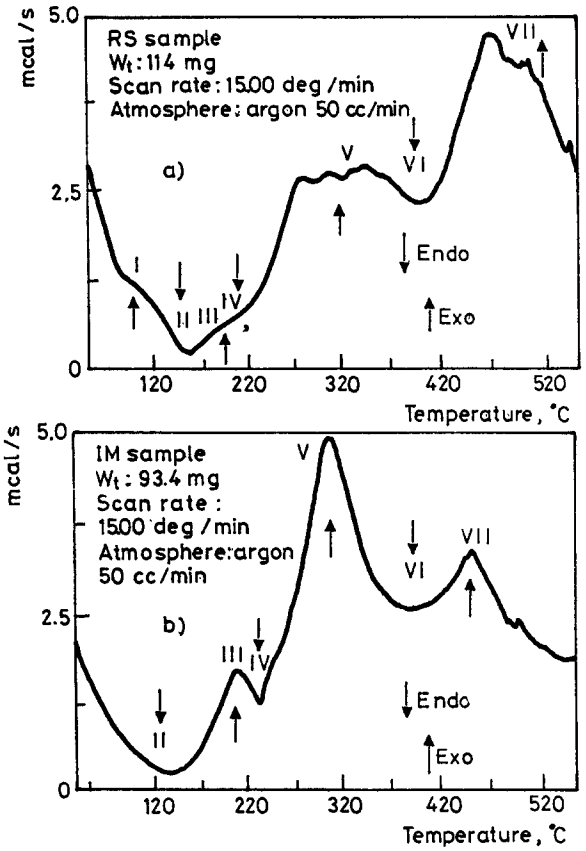

Fig. 2 a) DTA curve, heating rate: 15 deg·min^{-1}, in argon atmosphere, of the RS sample: as-atomized Al–2.3 Li–6.5 Mn in wt%) powders sieved in the <45 μm fraction size
b) DTA curve, heating rate: 15 deg·min^{-1}, in argon atmosphere, of the IM sample: conventionally cast Al–2.3 Li–6.5 Mn (in wt%) alloy
Identification of the exo- and endotherm peaks:
- (I) precipitation and (II) dissolution of the metastable (GP) AlLi phase;
- (III) precipitation of the δ' (Al_3Li) phase;
- (IV) dissolution of the δ' phase;
- (V) precipitation and (VI) dissolution of the δ phase;
- (VII) decomposition of the Al_6Mn phase

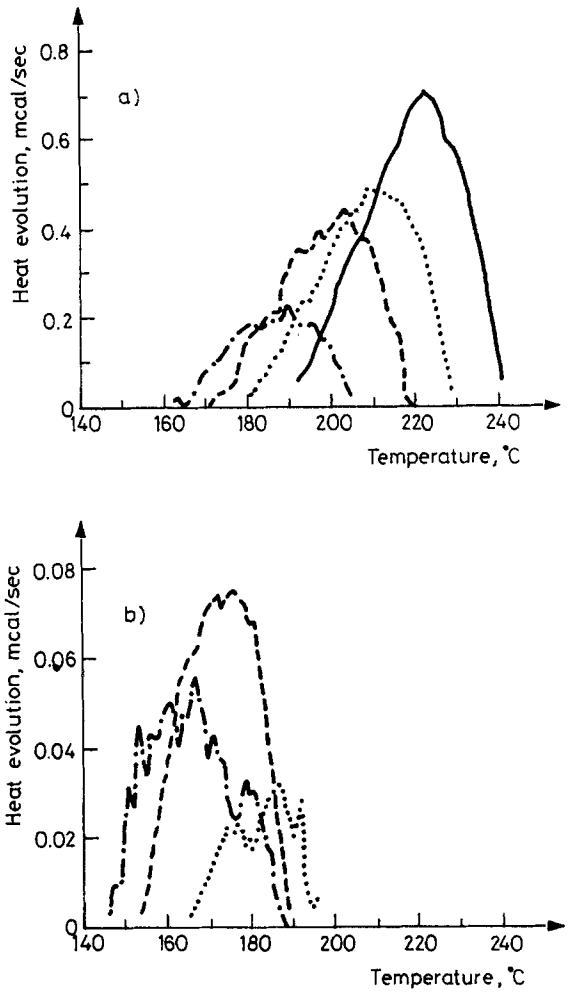

Fig. 3 a): Heat evolution rate ($mcal \cdot s^{-1}$) for the δ' (Al_3Li) phase precipitation, sample RS: as-atomized Al–2.3 Li–6.5 Mn (in wt%) powders, sieved in the <45 μm fraction size, b): Heat evolution rate ($mcal \cdot s^{-1}$) for the δ' (Al_3Li) phase precipitation, sample IM: conventionally cast Al–2.3 Li–6.5 Mn (in wt%) alloy

tinuous decomposition, with raising temperature, of the αAl–Mn solid solution also contributes to the continuous increase in heat capacity. As the heat treated samples have shown, no recrystallization takes place in this alloy, due to the presence of manganese [4]. All additional solid state transformations, including the 'GP' phase formation in this AlLi alloy, are discussed elsewhere [25].

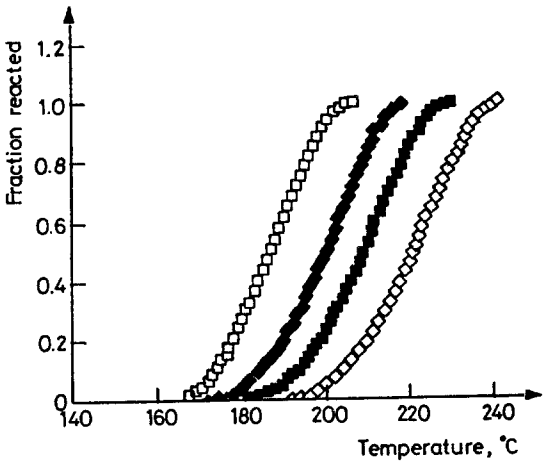

Fig. 4 a): Fraction of the δ' (Al_3Li) phase reacted *vs.* temperature, sample RS: as-atomized Al–2.3 Li–6.5 Mn (in wt%) powders, sieved in the <45 μm fraction size;

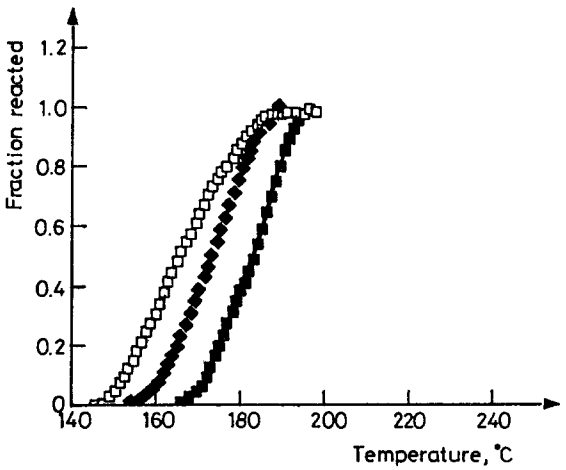

Fig. 4 b): Fraction of the δ' (Al_3Li) phase reacted *vs.* temperature, sample IM: conventionally cast Al–2.3 Li–6.5 Mn (in wt%) alloy

The heat evolution rate (in $mcal \cdot s^{-1}$) related to the δ' (Al_3Li) phase precipitation (peaks III in the thermograms), at the practiced heating rates, is shown in Figs 3a (RS sample) and 3b (IM sample). On those figures, one sees a significant decrease of the heat evolution rate in the RS samples as compared to the IM samples (notice the vertical scale changes in the graphs). The calculated enthalpy changes ΔH(in $cal \cdot g^{-1}$) shows the same trend, as seen in Table 1. This is an indication that the specific amount (per

unit weight of the material) of the δ' (Al_3Li) phase precipitated is lower in the RS sample than in the IM sample. Table 1 also lists the temperatures T_p and the crystallized fractions α_p evaluated at the tip of the peaks of the thermograms. The increase of T_p with increasing heating rate β is of course due to the kinetic nature of the both precipitation processes. The variation of the fraction reacted (precipitated) with temperature, at each practiced heating rate, is shown in Figs 4a and b. The temperatures at which the fraction reacted is $\alpha = 0.5$, as well as the peak temperatures, are systematically higher in the IM samples than in the RS samples, by 30° and more for peak III. This is an indication that the precipitation of the δ' (Al_3Li) phase occurs more readily in the rapidly solidified samples than in the conventionally cast one.

Table 1 Thermal analysis data

β	5 deg·min^{-1}	10 deg·min^{-1}	15 deg·min^{-1}	20 deg·min^{-1}
		RS Sample		
T_p, °C	167	175	187	–
ΔH, cal·g^{-1}	0.19	0.11	0.04	–
α_p	0.55	0.64	0.71	–
		IM Sample		
T_p, °C	190	204	212	223
ΔH, cal·g^{-1}	0.92	0.77	0.65	0.62
α_p	0.63	0.63	0.59	0.57

As stated above, the Kissinger method [16-17] has been applied to the study of the activation energy for the δ' (Al_3Li) phase precipitation, using data gained from heating runs at various heating rates β (5-20 deg·min^{-1}). The Kissinger plots are shown in Fig. 5, with their linear regression best fits. The slope of the straight lines in the semi-logarithmic plots $\left[\ln(\beta \cdot T_p^{-2}) \text{ vs. } T_p^{-1}\right]$ gives the ratio of the transformation (precipitation) activation energy E to the rate parameter n, $E \cdot n^{-1}$ [14]. The computed results are shown in Table 2. In order to assess for the effective activation energies E, the kinetic rate parameter n has been evaluated by the procedure explained in Section II, for the runs conducted at 5 deg·min^{-1}, the lowest heating rate, and for which the parameter α_p is indeed $\cong 0.633$, as requested for the validity of the model [18]. The activation energies are

77 kJ·mol^{-1} for the rapidly solidified sample ($n = 1.20$), and 105 kJ·mol^{-1} for the conventionally cast sample ($n = 1.37$), see Table 2. It should be noted that the $E \cdot n^{-1}$ value of 76.7 kJ·mol^{-1} for the IM sample is close to 80-83 kJ·mol^{-1}, the value reported for an Al–Li–Mg alloy [26]. Both values are however lower than the activation energy for diffusion of lithium in aluminum, 119 kJ·mol^{-1} [26]. Ref. [27] reports an activation energy of 108 kJ·mol^{-1} for a natural aged 8090 (Al–Li–Cu–Mg) alloy, with a rate parameter of 0.90.

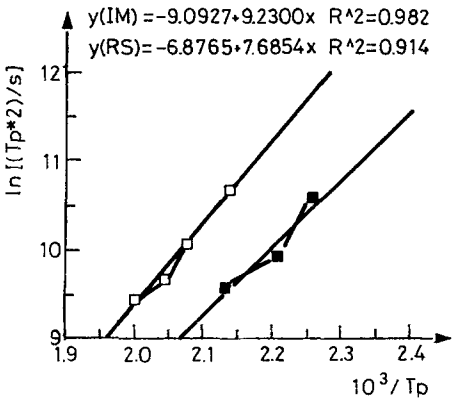

Fig. 5 Kissinger plots and best fits:
– sample RS: as-atomized Al–2.3 Li–6.5 Mn (in wt%) powders, sieved in the <45 μm fraction size; best fit: $y(RS) = -7.3311 + 7.9920x \cdot R^2 = 0.978$;
– sample IM: conventionally cast Al–2.3 Li–6.5 Mn (in wt%) alloy; best fit: $y(IM) = -9.0927 + 9.2300x \cdot R^2 = 0.982$

In the present study, the conventionally cast specimen (sample IM) shows higher activation energy for the precipitation of the δ' (Al_3Li) phase, as compared to the rapidly solidified RS specimen. There is a definite trend for lowering the activation energies for precipitation, as the quenching rate rises. This is attributed to the elastic strains generated in the aluminum matrix, due to the excess amount of manganese in solid solutions, consecutive to the high quenching rate practiced in rapid solidification. The rate parameter is apparently also influenced by that internal state of strain. It is known that strain gradients due to dislocations for example, do enhance precipitation in general, and the formation of the δ' (Al_3Li) phase in particular. The partial molar free energy of solute lithium atoms (atomic radius 2.05 Å), associated with a tensile stress in an aluminum (atomic radius 1.82 Å) matrix, is reduced at the vicinity of dislocations. As a result, lithium atoms drift toward dislocations, and precipitation is enhanced. This effect

has indeed been observed in the alloy studied, during aging experiments performed with and without prior mechanical stretching of the specimens [7]. Manganese has an atomic radius of 1.79 Å, slightly smaller than that of aluminum. The state of stress around each solute atom in a solid solution can be roughly evaluated by the misfit elastic energy theory [28]. This state of stress is a uniform hydrostatic pressure (or tension) given by:

$$p = 3K_{Mn}\,\varepsilon\left(\frac{3K_{Mn}}{3K_{Mn} + 4\mu_{Al}} - 1\right) \qquad [10]$$

where K_{Mn} is the bulk modulus of manganese, μ_{Al} is the shear modulus of aluminum and ε (positive or negative) is the misfit parameter $\{r^{\circ}_{Mn} = (1+\varepsilon)\cdot r^{\circ}_{Al}\}$. Applying the values listed for pure aluminum, lithium and manganese, yields the following results for the states of stress: $p_{Mn\,in\,aluminium}$: $+1.35\cdot 1010$ dyne·cm–2 and $p_{Li\,in\,aluminium}$:$-3.70\cdot 10^{10}$ dyne·cm^{-2}, a positive pressure in the aluminum matrix near the manganese atoms and a negative pressure in the aluminum matrix near the lithium atoms. It appears therefore that extended solid solution of manganese in aluminum may indeed induce strain gradients analogous to those produced by dislocations. The effect of such gradients, (the size of which is proportional to the solute atomic fraction [28]), is to enhance lithium precipitation, by lowering the activation energy, as observed, and also by affecting the rate parameter. The study of the kinetics of drift to dislocations [10] shows that the rate parameter for such a stress-assisted precipitation is 2/3, i.e. less than the computed value of 1.37. If, like in the case presented here, internal stresses are effective in the precipitation process, the overall observed rate parameter should indeed decrease, in correlation with the increase of the strain gradients induced by the solid solubility extension of manganese in the aluminum matrix. This is what is actually observed too.

Table 2 Activation energies and rate parameters

	$E\cdot n^{-1}$, kJ·mol^{-1}	n	E, kJ·mol^{-1}
RS sample	63.9	1.20	77
IM sample	76.7	1.37	105

A separate study has been undertaken in order to ascertain the existence and the value of any strain energy induced by the excess solid solubility of manganese in the rapidly solidified AlLiMn alloy, using an X–ray diffraction [29]. In this study, it has been shown that solute manganese atoms in the rapidly solidified Al–2.3 Li–6.5 Mn powders cause significant static displacement of the aluminum matrix atoms. The total (thermal and static) mean quadratic displacement was found to be 4.288 nm^2, instead of 3.00 nm^2 for pure aluminum, or for a perfectly annealed AlLiMn sample. The root mean square static displacement induced by excess manganese in aluminum is 1.099 nm, much greater than might have been expected from simple atomic misfit, and much greater also than those expected from a maximum concentration of quenched-in vacancies, as caused by rapid quenching. The corresponding elastic strain has evaluated to be: $2.692 \cdot 10^{-3}$, i.e. about 0.27%. It follows that the specific strain energy associated with the distorted lattice, calculated with the elastic bulk modulus of aluminum at room temperature: $7.31 \cdot 10^{10}$ Pa, attains the value of $2.65 \cdot 10^5$ $J \cdot m^{-3}$. This value is equivalent to the strain energy U that would have been introduced in the aluminum alloy by a dislocation density $\rho = 2.30 \cdot 10^4$ m^{-2}. Such a high value of the strain energy induced by the excess manganese solid solubility in the aluminum matrix is a manifestation of the metastable situation caused by the rapid quenching of the alloy. As such, it has a significant impact upon the precipitation kinetics of the third alloying element (lithium) present in the studied alloy. The strain gradients induced in the aluminum matrix, around the manganese atoms, by the extended manganese solid solution are indeed the reason why δ' (Al_3Li) precipitation in the rapidly solidified alloy is enhanced, and the activation energy for δ' precipitation lowered. The eventuality than there is a long range order in rapidly solidified Al–Mn alloys is now under investigation.

Conclusion

The extension of the manganese solid solubility beyond the thermodynamic equilibrium value induced by rapid solidification in an Al–Li–Mn alloy generates stress gradients within the aluminum matrix, that influences the precipitation kinetics of the metastable δ (Al_3Li) phase. Thermal analysis procedures have shown that the activation energy for precipitation is lowered, from 105 $kJ \cdot mol^{-1}$ for the conventionally cast material, down to 77 $kJ \cdot mol^{-1}$ for the sample that exhibits manganese solid solubility exten-

sion of 6.00 wt%. The observed enhancement of the δ (Al_3Li) phase precipitation is analogous to the well known δ' precipitation enhancement induced by dislocations. The rate parameter for the precipitation reaction is affected by the strain gradients too. Its value is reduced from about 1.40 to 1.20, as a result of the competing mechanisms involved in the δ' (Al_3Li) phase precipitation.

* * *

The alloy processing has been done at the Rapid Solidification Processing Laboratory, Materials Engineering Department, Ben–Gurion University of the Negev. JB gratefully acknowledges the support of a Grant–in–Aid (No. 3292/84) by the US.–Israel Binational Science Foundation.

References

1 Al-Li Alloys, edited by E. A. Starke and T. H. Sanders, Warrendale, PA : TMS-AIME, 1981.
2 Al-Li Alloys II, edited by E. A. Starke and T. H. Sanders, Warrendale, PA : TMS-AIME, 1984.
3 Al-Li Alloys III, edited by E. A. Starke and T. H. Sanders, Warrendale, PA : TMS-AIME, 1987.
4 H. Jones, Aluminium, 54 (1978) 274.
5 B. Noble and G. E. Thompson, Metals Science Journal, 5 (1971), 114.
6 E. A. Starke, T. H. Sanders and I. G. Palmer, Journal of Metals, 33 (1981) 24.
7 M. Ruhr, I. Ucok, E. Lavernia and J. Baram, in Light-Weight Alloys for Aerospace Applications, Proceedings of a Symposium sponsored by the TMS Nonferrous Metals Committee, held during the 1989 TMS annual Meeting, Las Vegas, Nevada, 1989, p. 79.
8 M. Ruhr, E. Lavernia and J. Baram, Metallurgical Transactions, 21A (1990) 1785.
9 J. Malek and J. Klikorka, J. of Thermal Anal. 32 (1987) 1883.
10 J. Burke, The Kinetics of Phase Transformation in Metals, Pergamon Press, 1965, p. 192.
11 M. Avrami, J. of Chemistry and Physics, (1939) 1103 and 8 (1940) 212.
12 W. A. Johnson and R. F. Mehl, Transactions of the A.I.M.E., 135 (1939) 416.
13 L. V. Meisel and P. J. Cote, Acta Metallurgica, 7 (1983) 1053.
14 D. W. Henderson, J. of Non-Crystalline Solids, 30 (1979) 301.
15 M. E. Brown and C. A. R. Phillpotts, J. of Chemical Education, 55 (1978) 556.
16 H. F. Kissinger, J. Res. Ntn. Bur. Std., 57 (1957) 217.
17 H. F. Kissinger, Analytical Chemistry, 29 (1957) 1702.
18 J. Malek, Thermochim. Acta, 138 (1989) 336.
19 W. L. Philips, J. of the Institute of Metals, 69 (1943) 275.
20 T. Ohashi, L. Dai and N. Fukatsu, Metallurgical Transactions, 17A (1986) 799.
21 E. J. Lavernia, E. Gutierrez, J. Sekely and N. J. Grant, International Journal of Rapid Solidification, 4 (1988) 125.
22 R. Nozato and G. Nakai, Tranactions J. I. M., 18 (1977) 679.
23 D. B. Williams and J. W. Edington, Metal Science, 9 (1975) 529.
24 D. Shechtman, R. J. Shaeffer and F. S. Biancaniello, Metallurgical Transactions 15A (1984) 1987.
25 A. Sembira and J. Baram, work in progress.
26 H. Jo, T. Ohshima and K. Hirano, Thermochim. Acta, 92 (1985) 309.
27 J. M. Badia, R. Servent and J. M. Antoraz, presented at the International Conference on Light Metals, Advanced Aluminum and Magnesium Alloys, Amsterdam, June 1990.

28 J. W. Christian, in The Theory of Transformations in Metals and Alloys, 2nd Edition, Part 1, Pergamon Press, 1975, p. 198.
29 J. Baram and L. Zevin, Scripta Materialia, accepted for publication.

Zusammenfassung — Es wird die Präzipitationskinetik der '(Al_3Li) Phase in zwei schnell erstarrten und einer gewöhnlich gegossenen Probe einer Al-2.3Li-6.5Mn (in Gew.%) Legierung miteinander verglichen. Bei hohen Abkühlgeschwindigkeiten wird Mangan in der Aluminiummatrix (Al) bis zu 6.0 Gew.% als feste Lösung zurückbehalten, weit über den thermodynamischen Gleichgewichtswert (0.36 Gew.% bei 500°C) hinaus. Derart ausgedehnte feste Lösungen von Mangan in Aluminium erzeugen Spannungsgradienten, ähnlich wie die durch Versetzung hervorgerufen. Die Wirkung solcher Gradienten, deren Größe sich proportional zum gelösten Atombruch verhält, steigert, wie beobachtet durch Minderung der Aktivierungsenergie und auch durch Beeinflussung des Geschwindigkeitsparameters die Präzipitation von Lithium. Die kinetische Thermoanalyse wurde mittels einer Reihe von nichtisothermen DTA-Versuchen durchgeführt. Die Präzipitation der '(Al_3Li) Phase wird durch einen exothermen Peak bewiesen, dessen Charakteristik analysiert wurde. Die Geschwindigkeit der Umwandlung (Präzipitation) scheint der Johnson-Mehl-Avrami-Gleichung zu unterliegen. Aktivierungsenergie des Präzipitationsvorganges als auch der Geschwindigkeitsparameter wurden sowohl für schnell verfestigte als auch für gewöhnlich gegossenen Proben ermittelt. Die Aktivierungsenergie für die Präzipitation wird von 105 $kJmol^{-1}$ für das gewöhnlich gegossene Material auf einen Wert von 77 $kJmol^{-1}$ für eine Probe mit einem gelösten Mangangehalt von 6.00 Gew.% gesenkt. Der Geschwindigkeitsparameter für die Präzipitationsreaktion wird von etwa 1.40 für die langsam gegossene Probe auf 1.20 für die schnell verfestigten Proben gesenkt.